ICIC Express Letters
Volume **18**, Number **5**, May **2024**

 ISSN 1881-803X
pp. **423–432**

AUTOMATIC CARDIAC MRI CLASSIFICATION USING DEEP RESIDUAL NETWORKS

Dessy Irmawati[1,2,*], Oyas Wahyunggoro[1] and Indah Soesanti[1]

[1]Department of Electrical and Information Engineering
Universitas Gadjah Mada
Bulaksumur, Yogyakarta 55281, Indonesia
{ oyas; indahsoesanti }@ugm.ac.id

[2]Department of Electrical and Electronic Engineering
Universitas Negeri Yogyakarta
Jl. Colombo No. 1 Karangmalang, Yogyakarta 55281, Indonesia
*Corresponding author: dessy.irmawati@uny.ac.id

Received May 2023; accepted August 2023

Abstract. *Due to the excellent spatial resolution that cardiac magnetic resonance imaging (CMR) offers, it is possible to better extract crucial functional and morphological aspects for the staging of cardiovascular illness. CMR, with its great spatial resolution, allows for the improved extraction of crucial functional and morphological elements for the staging of cardiovascular disease. Cardiologists employ CMR to assess temporal geometric changes and manually estimate heart function by outlining forms. Yet, this work demands a great deal of accuracy and takes a long time. For cardiac analysis, deep learning techniques have been widely used. The stages proposed in this study include (i) converting 3-dimensional images into 2-dimensional ones, (ii) obtaining contour values from ground truth images, (iii) cropping the image localization area to obtain the region of interest (RoI), (iv) dataset separation to train, validate, and test data (70%, 20%, 10%), and (v) classify using the ResNet50 V2 model. The ACDC MICCAI 2017 dataset is used in this study to classify the cardiac into five main categories abnormal and one healthy the ResNet50 V2 architecture. By having a measurement accuracy of 0.98, performance outcomes are indicated. Experimental results show the robustness of the proposed architecture.*

Keywords: Cardiac classification, CMR, ResNet50, Deep learning

1. **Introduction.** CMR is a frequently used technique for diagnosing and treating cardiovascular disease. Since CMR has advanced, it may now be used to visualize the anatomy as well as offer accurate quantitative measurements of the myocardial, left ventricle, and right ventricle. CMR employs a computer-generated radio wave and a magnetic field to precisely assess a patient's heart state. Medical professionals' direct cardiac analysis still leaves a possibility of error in diagnosis. This is caused by a medical environment, where a radiologist manually draws contours around the structure of interest to separate it from the surrounding tissues from organs and the patient usually also does not perform early detection [1]. This approach, however, becomes impractical in a high throughput hospital since it is time-consuming, laborious, and adds intra and inter rater inconsistency [2]. CMR is a 3-dimensional greyscale image, which still contains many artifacts. Moreover, the cardiac images produced by a magnetic resonance imaging (MRI) machine still cover all parts of the heart, while detection of myocardial abnormalities is indicated from ventricle functional such as end-diastole volume (EDV), end-systole volume (ESV), ejection fraction (EF), and stroke volume [3].

DOI: 10.24507/icicel.18.05.423

Cardiologists still require computer assisted detection (CAD) to help them cut faults. It is challenging for experts to consistently provide a reliable and correct diagnosis due to the intricacy of CMR imaging and the wide range of variances among human experts. CMR imaging can show the state of the pathological alterations that take place, so that an abnormal cardiac can be predicted using the statistical features gleaned from CMR images. Fully convolutional networks which are based on deep learning, have found significant lead to powerful and the capacity to highly learn classification models. Convolutional neural networks (CNN), which are a very popular deep learning model, have had the most performance to further in the processing of medical images. CNN are specialized multilayers feed forward neural networks that are excellent for pattern classification. It was created with the specific purpose of identifying two-dimensional visual patterns in input images. Several publications on deep learning have been published since then about CMR analysis. Most articles sliced-by-sliced evaluated the MRI data using 2D CNN [4].

Currently, segmentation challenges generally require a ground-truth value as well as an evaluation matrix as a comparison [2]. In addition, CMR images are complex images and are accompanied by a lot of noise, which results in errors. Meanwhile, CMR image analysis for segmentation and classification has been summarized by Bernard et al. [4], where nine papers use the deep convolutional networks method with the U-Net like networks model for segmentation, which are in [5, 6, 7, 8, 9, 10, 11, 12, 13, 14]. Four papers use machine learning methods, including support vector machine (SVM) and random forest (RF) for CMR image classification, such as in [6, 8, 12, 15]. Most CMR image analysis methods for classification go through several stages, namely region of interest (RoI), segmentation, and classification. The original CMR image still contains a lot of information, so RoI is needed to limit the area, as well as speed up the computation process. The RoI image is then segmented to produce features for classification.

The aim of this paper is for end to end classifying CMR images using a residual network-based CNN model. ResNet architecture [16] has won the ImageNet challenge in 2015 known as ResNet-blocks. The deeper network has a higher test error as a result of higher training error [16], such that these issues can be solved by the residual block. Because the residual block does not learn a function; instead, it merely learns the residual, which preconditions it to learn mappings in each layer that are close to the identity function. This enables the efficient training of even deeper models [17].

The CNN model could produce feature maps generated at the convolution and pool layers, as well as classification at the fully connected layer. However, getting deeper into the network will worsen performance. Contributions to this paper are converting raw 4D images into 2D, then constraining the images to produce RoI images, and classifying the dataset with ResNet50 v2 pretrained residual networks. This article's motivation is the high accuracy that can be achieved when classifying cardiac MRI images using the ResNet50 v2 pre-trained model.

The rest of this essay is structured as follows. The next section will present some related CMR image analysis research. The dataset used for our studies is described in the section that follows, along with the processes used in the experiments to prepare the raw dataset for classification in the model. The section that follows presents the classification results using the pretrained ResNet50 v2 validation set and test set. The final section concludes the research.

2. **Related Work.**

Some researchers [2, 6, 18, 19, 20, 21, 22] perform segmentation to start the classification process. Table 1 shows that most researchers used a deep learning model and modified it to process a segmentation CMR. Ensemble of classifier was applied for segmented image classification by Khened et al. [2], while other researchers used classification diagnosis network using permutation invariant network [7], 4 ridges logistic regression binary model [8], and dual attention mechanism [9]. CardiacCN unsupervised

Table 1. Summary of cardiac MRI challenge for MRI image analysis

Reference	Method
Segmentation and Classification Challenges	
Khened et al. [2]	Segmentation using DenseNet based FCN architecture. Ensemble of classifier (RF, MLP, SVM, Naïve Bayes) for classification
Chang et al. [18]	Segmentation using FCN and Classification Diagnosis Network using permutation invariant network
Zheng et al. [19]	Segmentation using LVRV-net (variant of U-net) and 4 ridges logistic regression binary model for classification
Ding et al. [20]	Segmentation using Pretrained VGG16 and Classification network based on dual attention mechanism to classify the dataset
Ammar et al. [21]	Segmentation using UNet fully convolution neural network variant. Classified by ensemble classifier (MLP, RF, and SVM)
Isensee et al. [6]	Ensemble of UNet used to segment the cardiac structures (LVC, RVC, and LVM). The features are trained using ensemble classifier (MLP and RF)
Classification Challenges	
Xie et al. [22]	CardiacCN unsupervised domain adaptive for classification
Maruyama et al. [23]	Three types of machine learning (SVM, ANN, and CNN) were used to classify the dataset where in different format (JPEG and DICOM)
Extraction and Prediction Challenges	
Ho and Kim [26]	MobileNet (CNN) to extract and LSTM (RNN) to predict

adaptive domain [9] was applied to myocardial infarction (MINF) classification as the answer to ineffective and prone to error during medical treatment using MRI. The best results were obtained in four out of the seven evaluation criteria in the study [26], which used MobileNet as a feature extractor fitted with predictors in the form of a two-layer long short-term memory (LSTM) network. Evaluation of several classification models for multi-class classification has also been done [13]. Other researchers compared the accuracy of the classification results of machine learning (SVM and ANN) with CNN using two types of CMR image data (JPEG and DICOM), and CNN showed more accurate results than machine learning [12]. The study's findings are presented in Table 1: [18] uses cardiac point clouds with 3D convolutional operation, [22] employs adaptable networks for classification models, [23] contrasts three machine learning approaches for classification, and [19] uses four classifiers that are assembled. Although these studies have several flaws, the outcomes of segmentation to produce characteristics often make it harder to diagnose heart pathologies.

3. Materials and Methods.

3.1. **Overview.** Figure 1 shows the process flow of the suggested technique. Pre-processing and classification are the two stages that are completed. The method shown in Figure 1 includes (i) pre-processing, which entails transforming Cine MRI 3D pictures into 2D images for the data-preparation step, then (ii) processing the images to produce RoI images. To assess the effectiveness of deep learning models, the dataset is divided into three sections: sections for training, validation, and testing; finally (iii) disease prediction classifier used for classification in addition to deep learning based residualnet classifiers for disease prediction.

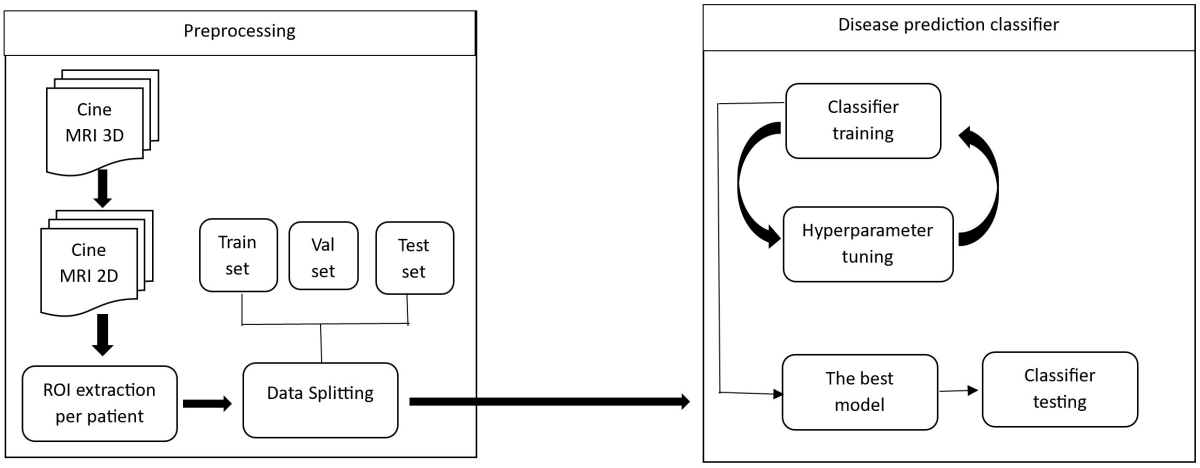

FIGURE 1. Preprocessing (left) and prediction (right) workflow

3.2. **Preparation of data.** Cine MRI 3D is made up of raw data from two MR scanners at the University Hospital of Dijon that were used to analyze the MICCAI ACDC 2017 dataset (1.5 T and 3.0 T). The ACDC training set and testing set are each separated into five equal-sized groups. The groups consist of four pathological subjects and one healthy subject patient, those data available on website, as follows: (i) NOR-normal subjects, (ii) MINF-myocardial infarction, (iii) DCM-dilated cardiomyopathy, (iv) HCM-hypertrophic cardiomyopathy, and (v) RV-abnormal right ventricle.

Examining the train, validation, and test sets of the given cine MRI image dataset revealed distinct variations (height/weight). Pre-processing stage after converting CMR 3D to 2D, we got variations of dimension of images. In this study, the images should be cropping to square area to get RoI images.

MICCAI ACDC 2017 provides 100 short-axis-cine CMR patients for training data and 50 for tests. However, the groundtruth (GT) value is only available in the training data. This GT value is useful for measuring contours, namely x, y, and h. Contour calculation begins with the GT image thresholding, then normalization is carried out, and calculating the contour value for the original image crop. The whole process is shown in Figure 2, and the original normalized image is then bounded by the contours obtained from the calculation of the GT image. The boundary area is then cropped to produce an RoI image.

3.3. **Network architecture.** Deep CNN networks are generally acknowledged to be able to resolve classification issues with many input images. The CNN network is interwoven with layers that may create features, while the more features there are, the deeper the layer remains [24, 25]; therefore, deep learning methods can automatically learn features for classification. However, deep learning can experience poor performance when vanishing, overfitting, and underfitting problems occur. The weakening in training accuracy shows that not all systems are equally amenable to optimization. The suggested method is a deep residual network with residual blocks in which signals may be directly transmitted from one block to another when there exist identical mappings as skip connection [16]. Construction of deep learning by adding layer of identity maping can resolve the weakening of deeper model. Figure 3(a) shows the residual block, where $F(x) + x$ can be easier to optimize the residual mapping. Deep learning model ResNet50 was used in training along, by no-trainable layer or well-known as pre-trained deep learning. Deep residual networks have components that can transmit information directly throughout the entire network as well as between residual units [16]. Residual network (ResNet) is a deep convolution network that has a shortcut connection in the form of a skip block which is called a

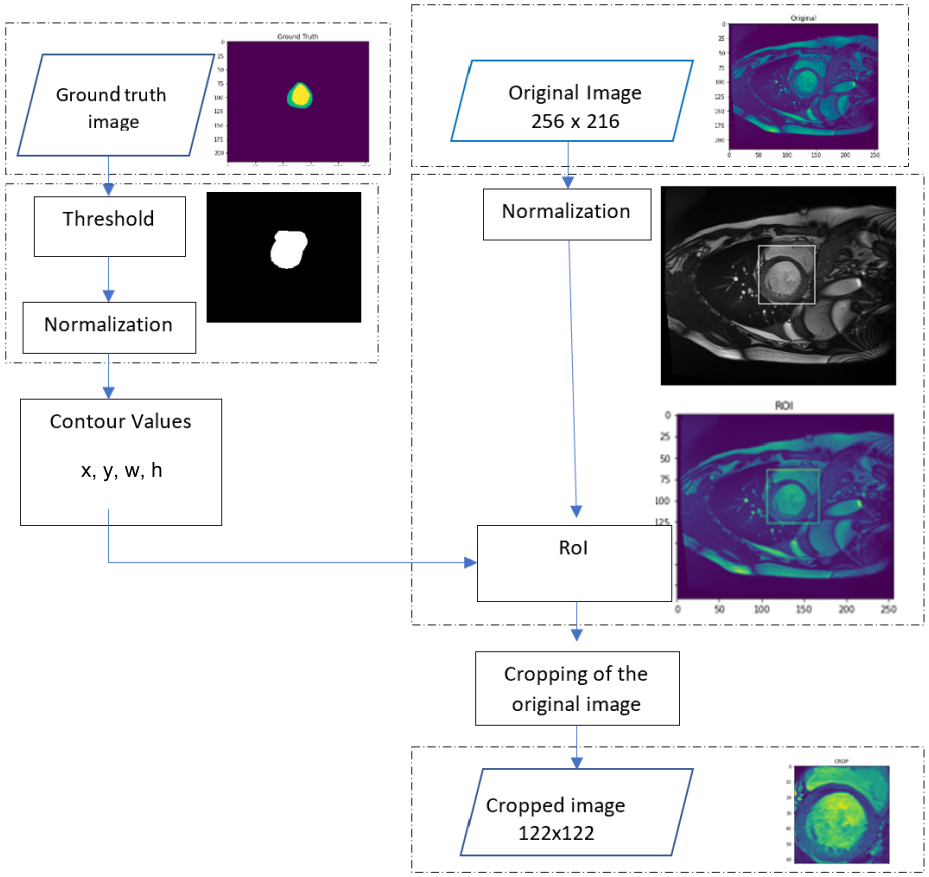

FIGURE 2. Cropping image processing

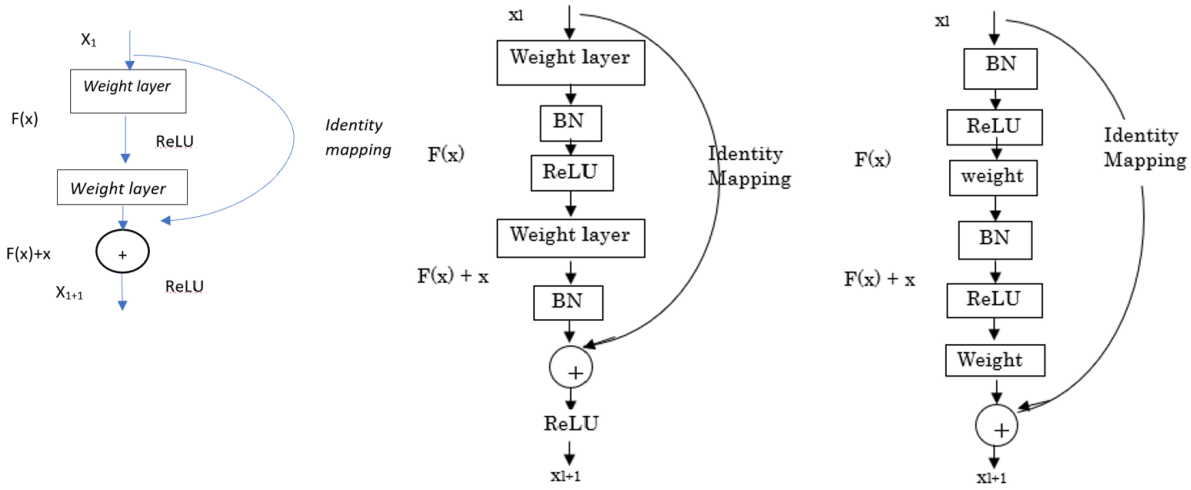

(a) (b) (c)

FIGURE 3. Variant of identity mapping: (a) The residual block, (b) identity mapping with post-activation, and (c) identity mapping with pre-activation

bottleneck. This block has two types of designs, namely for the same feature map output, then the layers have the same number of filters, whereas if the feature map size is half the size smaller, then the number of filters is multiplied by two. Based on Figure 3(a), it is stated that the lth input is x_l and the output is x_{l+1}. F is the residual function and $h(x_l) = x_l$ is the identity map. Figure 3(a) has identity mapping structure, with

ReLU and BN as weight layer pre-activation. These structures allow for extensive use of the network depth dimension, which is essential to the success of current deep learning [5]. The post-activation structure produces a poor test for deeper layers, while the pre-activation structure allows adjusting the number of layers until it reaches convergence with light training. A comparison of the two identity mapping variants in different structures are shown in Figures 3(b) and 3(c). The ResNet50 model with identity Mapping pre-activation is shown in Figure 3(c), known as ResNet50 V2.

The extensive training makes it easier to build deeper networks and provides improved accuracy. Figure 4 depicts the ResNet50 network, which has a 7 by 7 receptive field and is 50 layers deep, and then this is followed by a max-pooling layer with a kernel size of 3×3. In deep learning, computer models learn to perform classification tasks directly from images. Models are taught by large amounts of labeled data with deep learning architectures. During deep learning training, it is necessary to have a mechanism to prevent over-learning from training data and subpar performance after deployment in production. The training set, validation set, and test sets are formed by dividing the 2D CMR image data into three sets (70 : 20 : 10) during the RoI technique. Therefore, this process can determine how well the model generalizes, prevent the model from overfitting, and effectively evaluate the model. Figure 5 shows a graph of the distribution of the datasets.

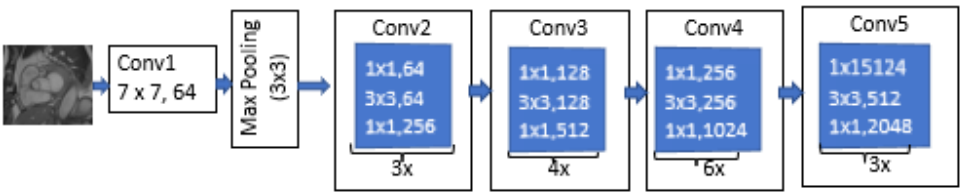

FIGURE 4. Block diagram of ResNet50

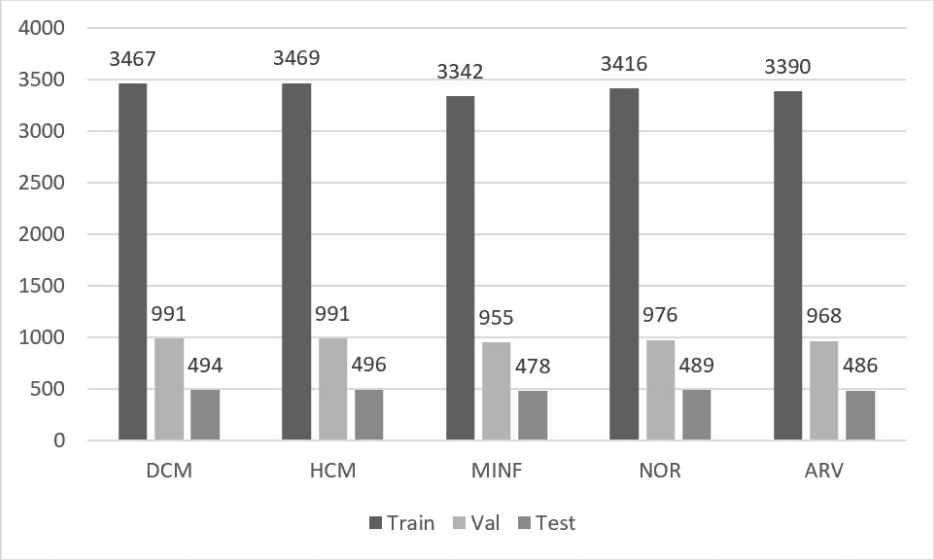

FIGURE 5. Distribution of splitting data

CMR images were trained using the ResNet50 V2 pre-trained model into five classes (DCM, HCM, MINF, NOR, and AV). The total data used were 24408 CMR 2D, 17084 training sets, 4881 validation sets and 2443 test sets. The number of epochs in the trained model is 50, minimizing the model error using the ADAM optimizer with a learning rate of 10^{-3}. Setting the learning rate α is very important before conducting training, how far the weight transfer reaches the minimum global area is determined by the magnitude

of learning rate. If the value of the learning rate parameter is too large, it will cause the model training to not converge or exceed the minimum area, but if it is too small, then the training will be better, but it will be slow. The relationship between gradient descent and learning rate is given in Equation (1).

$$\Theta_{new} = \Theta_{old} - \alpha \cdot \nabla \jmath(\Theta_{old}) \tag{1}$$

The ResNet50 V2 base model was trained using weights from ImageNet training (pre-trained). Freezing layers are activated during training, so the weights are not updated and then the best weight is used for classification. The classification training process chart is shown in Figure 6.

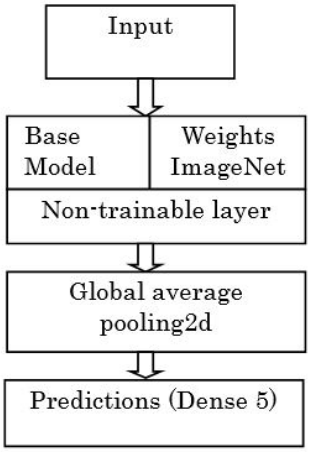

FIGURE 6. Block diagram of training

4. **Result and Discussion.** The training and validation loss values offer a better understanding of how the learning performance changes throughout the number of epochs and aid in the diagnosis of any learning issues that may result in an underfit or an overfit model, which is why they are crucial pieces of information. They are additionally going to offer researchers with information on the epoch for the inferencing stage, which will employ the learned model weights. When the model is overly simplistic, undefitting occurs. In the training data, the model will not be able to recognize key patterns. It therefore performs poorly on both training and validation data. While too much complexity in the model can lead to overfitting. Instead of learning patterns, the model has an ability to retrain the training data. As a result, it performs well with training data but poorly with previously unexplored data. As a result, the model is unable to generate new data. More data samples will aid in preventing overfitting in the model. In the best case scenario or good fit, the model recognizes patterns in the training data and generalizes well to new, untried data without underfitting or overfitting. Figure 7(a) displays the training outcomes; the training data movement (dotted line) advances to epoch 50, the final epoch, with improved accuracy and convergence at 1. The same is true for Figure 7(b)'s validation data movement; a small difference between values and a training and validation loss that decreases to a stable level signify a successful match. The loss of the model will almost always be smaller on the training dataset than on the validated dataset.

The confusion matrix of model is provided in Figure 8. The confusion matrix indicates can distinguish well every case. There is a misclassification under 0.05 between ARV and NOR case. Formulas of Precision, Recall, F1-Score, and Accuracy are given in Equations (2)-(5) and those represent the performance evaluation of the model in predicting each case as shown in Table 2, where performance results obtained successively 0.98.

$$Precision = \frac{TP}{TP + FN} \tag{2}$$

$$Recall = \frac{TP}{(TP + FN)} \tag{3}$$

$$Accuracy = \frac{TP_A + TP_B + TP_C + TP_D + TP_E}{\Sigma TP + \Sigma E} \tag{4}$$

$$F1 = \frac{2 \times precision \times recall}{precision + recall} \tag{5}$$

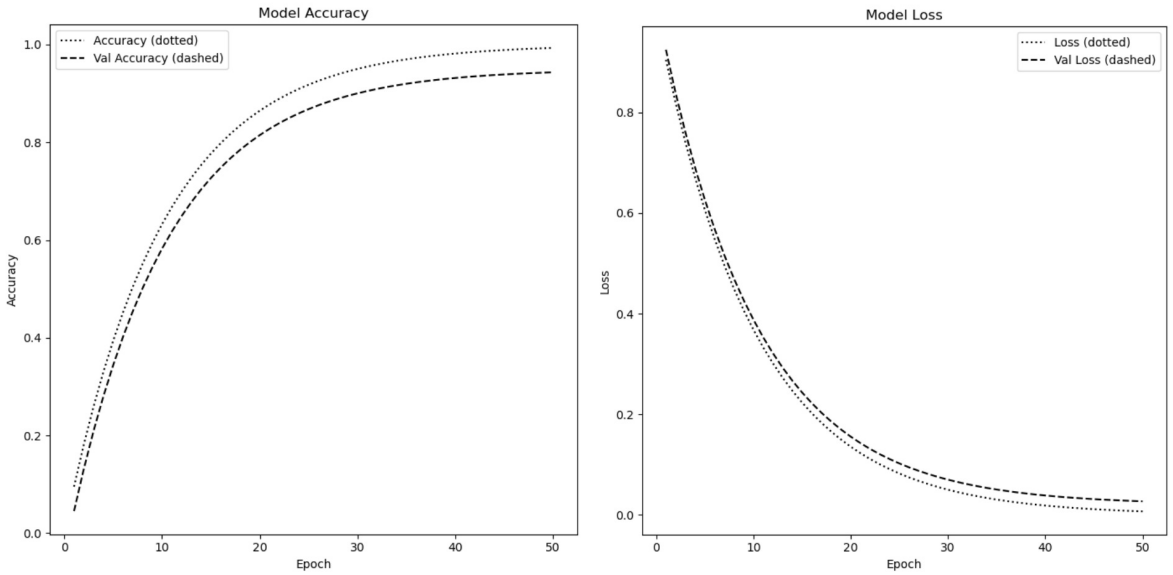

(a) (b)

FIGURE 7. Graph of accuracy (a) and loss (b)

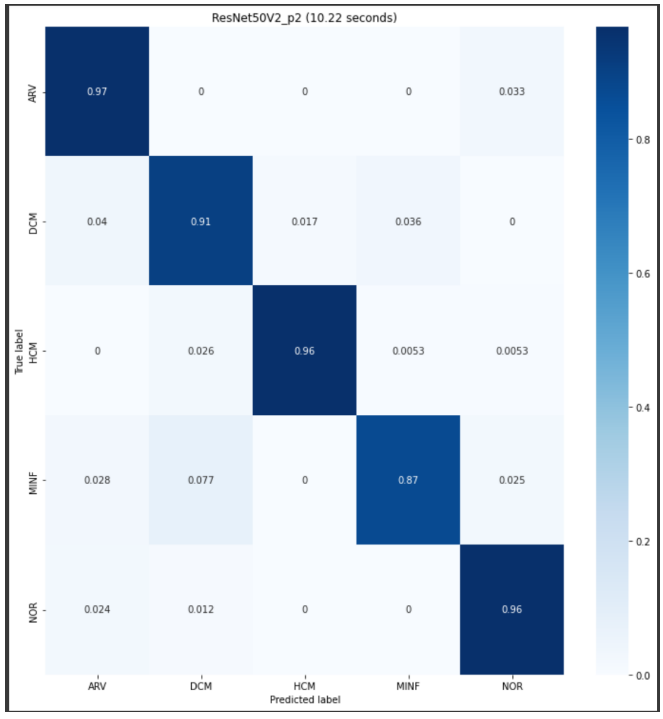

FIGURE 8. Confusion matrix of the classification

Table 2. Evaluation result for baseline model

	Precision	Recall	F1-Score	Number of data
ARV	0.98532	0.96708	0.97612	486
DCM	0.99798	0.99798	0.99798	494
HCM	0.99798	0.99697	0.99697	496
MINF	0.99167	0.99374	0.99374	478
NOR	0.96781	0.97566	0.97566	489
Accuracy			0.98813	2443
Macro avg	0.98815	0.98810	0.98809	2443
Weighted avg	0.98819	0.98813	0.98813	2443

5. **Conclusions.** Computing load and misclassification, can be anticipated by converting 4D images to 2D and localizing images to RoI. In comparison to earlier research using distinct feature extraction steps, end to end pretrained ResNet can generate performance with 98% more accuracy. The model can classify 5 classes (DCM, HCM, MINF, NOR, and ARV). This research still contains limitations and still needs to be tested on the model, so that the model can be generalized to other CMR image dataset.

Acknowledgment. The Indonesia Endowment Funds for Education (LPDP) are helping to fund a portion of this project. We would like to convey our sincere gratitude to our supervisor team, Oyas Wahyunggoro, Ph.D., and Dr. Indah Soesanti, for their unflagging support and direction throughout the research process. Their knowledge, perspective, and support were crucial in enabling us to finish this assignment.

REFERENCES

[1] R. L. B. Buana and I. Hudati, Review: Analysis of arrhythmia detection features and deep learning methods for wearable devices, *National Journal of Electrical Engineering and Information Technology*, vol.11, no.1, pp.61-69, DOI: 10.22146/jnteti.v11i1.3381, 2022.

[2] M. Khened, V. A. Kollerathu and G. Krishnamurthi, Fully convolutional multi-scale residual DenseNets for cardiac segmentation and automated cardiac diagnosis using ensemble of classifiers, *Med. Image Anal.*, vol.51, pp.21-45, DOI: 10.1016/j.media.2018.10.004, 2019.

[3] M. Muthulakshmi and G. Kavitha, Deep CNN with LM learning based myocardial ischemia detection in cardiac magnetic resonance images, *2019 41st Annual International Conference of the IEEE Engineering in Medicine and Biology Society (EMBC)*, Berlin, Germany, pp.824-827, DOI: 10.1109/EMBC.2019.8856838, 2019.

[4] O. Bernard, A. Lalande, C. Zotti et al., Deep learning techniques for automatic MRI cardiac multi-structures segmentation and diagnosis: Is the problem solved?, *IEEE Trans. Med. Imaging*, vol.37, no.11, pp.2514-2525, 2018.

[5] C. F. Baumgartner, L. M. Koch, M. Pollefeys and E. Konukoglu, An exploration of 2D and 3D deep learning techniques for cardiac MR image segmentation, in *Statistical Atlases and Computational Models of the Heart. ACDC and MMWHS Challenges. STACOM 2017. Lecture Notes in Computer Science*, M. Pop et al. (eds.), Cham, Springer, pp.111-119, 2018.

[6] F. Isensee, P. Jaeger, P. M. Full, I. Wolf, S. Engelhardt and K. H. Maier-Hein, Automatic cardiac disease assessment on cine-MRI via time-series segmentation and domain specific features, in *Statistical Atlases and Computational Models of the Heart. ACDC and MMWHS Challenges. STACOM 2017. Lecture Notes in Computer Science*, M. Pop et al. (eds.), Cham, Springer, pp.120-129, 2018.

[7] Y. Jang, Y. Hong, S. Ha, S. Kim and H. J. Chang, Automatic segmentation of LV and RV in cardiac MRI, in *Statistical Atlases and Computational Models of the Heart. ACDC and MMWHS Challenges. STACOM 2017. Lecture Notes in Computer Science*, M. Pop et al. (eds.), Cham, Springer, pp.161-169, 2018.

[8] M. Khened, V. Alex and G. Krishnamurthi, Densely connected fully convolutional network for short-axis cardiac cine MR image segmentation and heart diagnosis using random forest, in *Statistical Atlases and Computational Models of the Heart. ACDC and MMWHS Challenges. STACOM 2017. Lecture Notes in Computer Science*, M. Pop et al. (eds.), Cham, Springer, pp.140-151, 2018.

[9] J. Patravali, S. Jain and S. Chilamkurthy, 2D-3D fully convolutional neural networks for cardiac MR segmentation, in *Statistical Atlases and Computational Models of the Heart. ACDC and MMWHS Challenges. STACOM 2017. Lecture Notes in Computer Science*, M. Pop et al. (eds.), Cham, Springer, pp.130-139, 2018.

[10] M.-M. Rohé, M. Sermesant and X. Pennec, Automatic multi-atlas segmentation of myocardium with SVF-Net, in *Statistical Atlases and Computational Models of the Heart. ACDC and MMWHS Challenges. STACOM 2017. Lecture Notes in Computer Science*, M. Pop et al. (eds.), Cham, Springer, pp.170-177, 2018.

[11] E. Grinias and G. Tziritas, Fast fully-automatic cardiac segmentation in MRI using MRF model optimization, substructures tracking and B-spline smoothing, in *Statistical Atlases and Computational Models of the Heart. ACDC and MMWHS Challenges. STACOM 2017. Lecture Notes in Computer Science*, M. Pop et al. (eds.), Cham, Springer, pp.91-100, 2018.

[12] J. M. Wolterink, T. Leiner, M. A. Viergever and I. Išgum, Automatic segmentation and disease classification using cardiac cine MR images, in *Statistical Atlases and Computational Models of the Heart. ACDC and MMWHS Challenges. STACOM 2017. Lecture Notes in Computer Science*, M. Pop et al. (eds.), Cham, Springer, pp.101-110, 2018.

[13] X. Yang, C. Bian, L. Yu, D. Ni and P.-A. Heng, Class-balanced deep neural network for automatic ventricular structure segmentation, in *Statistical Atlases and Computational Models of the Heart. ACDC and MMWHS Challenges. STACOM 2017. Lecture Notes in Computer Science*, M. Pop et al. (eds.), Cham, Springer, pp.152-160, 2018.

[14] C. Zotti, Z. Luo, O. Humbert, A. Lalande and P.-M. Jodoin, GridNet with automatic shape prior registration for automatic MRI cardiac segmentation, in *Statistical Atlases and Computational Models of the Heart. ACDC and MMWHS Challenges. STACOM 2017. Lecture Notes in Computer Science*, M. Pop et al. (eds.), Cham, Springer, pp.73-81, 2018.

[15] I. Cetin, G. Sanroma, S. E. Petersen, S. Napel, O. Camara, M.-A. G. Ballester and K. Lekadir, A radiomics approach to computer-aided diagnosis with cardiac cine-MRI, in *Statistical Atlases and Computational Models of the Heart. ACDC and MMWHS Challenges*, M. Pop et al. (eds.), Cham, Springer, pp.82-90, 2018.

[16] K. He, X. Zhang, S. Ren and J. Sun, Identity mappings in deep residual networks, in *Computer Vision – ECCV 2016. ECCV 2016. Lecture Notes in Computer Science*, B. Leibe, J. Matas, N. Sebe and M. Welling (eds.), Cham, Springer, pp.630-645, 2016.

[17] G. Litjens, T. Kooi, B. E. Bejnordi, A. A. A. Setio, F. Ciompi, M. Ghafoorian, J. A. van der Laak, B. van Ginneken and C. I. Sánchez, A survey on deep learning in medical image analysis, *Med. Image Anal.*, vol.42, no.12, pp.60-88, 2017.

[18] Y. Chang, B. Song, C. Jung and L. Huang, Automatic segmentation and cardiopathy classification in cardiac MRI images based on deep neural networks, *2018 IEEE International Conference on Acoustics, Speech and Signal Processing (ICASSP)*, Calgary, AB, Canada, pp.1020-1024, 2018.

[19] Q. Zheng, H. Delingette and N. Ayache, Explainable cardiac pathology classification on cine MRI with motion characterization by semi-supervised learning of apparent flow, *Med. Image Anal.*, vol.56, pp.80-95, 2019.

[20] Y. Ding, W. Xie, K. K. Wong and Z. Liao, Classification of myocardial fibrosis in DE-MRI based on semi-supervised semantic segmentation and dual attention mechanism, *Comput. Methods Programs Biomed.*, vol.225, 107041, 2022.

[21] A. Ammar, O. Bouattane and M. Youssfi, Automatic cardiac cine MRI segmentation and heart disease classification, *Comput. Med. Imaging Graph.*, vol.88, no.12, 101864, 2021.

[22] W. Xie, Y. Ding, Z. Liao and K. K. Wong, Unsupervised domain adaptive myocardial infarction MRI classification diagnostics model based on target domain confused sample resampling, *Comput. Methods Programs Biomed.*, vol.226, 107055, 2022.

[23] T. Maruyama, N. Hayashi, Y. Sato, S. Hyuga, Y. Wakayama, H. Watanabe, A. Ogura and T. Ogura, Comparison of medical image classification accuracy among three machine learning methods, *J. Xray. Sci. Technol.*, vol.26, no.6, pp.885-893, 2018.

[24] K. He, X. Zhang, S. Ren and J. Sun, Deep residual learning for image recognition, *2016 IEEE Conf. Comput. Vis. Pattern Recognit.*, pp.770-778, 2016.

[25] S. Abd ElGhany, M. R. Ibraheem, M. Alruwaili and M. Elmogy, Diagnosis of various skin cancer lesions based on fine-tuned ResNet50 deep network, *Comput. Mater. Contin.*, vol.68, no.1, pp.117-135, 2021.

[26] N. Ho and Y.-C. Kim, Estimation of cardiac short axis slice levels with a cascaded deep convolutional and recurrent neural network model, *Tomography*, vol.8, no.6, pp.2749-2760, DOI: 10.3390/tomography8060229, 2022.